ELSEVIER

Journal of Power Sources 70 (1998) 240–246

JOURNAL OF POWER SOURCES

Calculation of temperature rise in lithium polymer batteries of Sandia conceptual designs during USABC Dynamic Stress Test

Yufei Chen [a], James W. Evans [a,*], Greg Scharrer [b]

[a] *Energy and Environment Division, Lawrence Berkeley National Laboratory, and Department of Materials Science and Mineral Engineering, University of California, Berkeley, CA 94720, USA*

[b] *Sandia National Laboratories, P.O. Box 5800, Albuquerque, NM 87185, USA*

Received 14 February 1997; revised 11 June 1997

Abstract

Based on reported galvanostatic charge and discharge data of a $Li/P(EO)_8LiClO_4/TiS_2$ cell, heat generation rates within a battery during the USABC Dynamic Stress Test (DST) were calculated and compared with those during the Simplified Federal Urban Driving Schedule (SFUDS) dynamic power profile. Also, calculations of temperature rise in the C/Polymer electrolyte/$LiMn_2O_4$ batteries of Sandia conceptual designs for a Ford van and GM Impact, during a DST/Fast Charge/DST/Full Charge cycle were conducted with a three-dimensional thermal model. © 1998 Elsevier Science S.A.

Keywords: Lithium polymer batteries; Dynamic stress test; Simplified federal urban driving schedule

1. Introduction

Safety issues associated with lithium batteries have, to a large extent, delayed the successful commercialization of rechargeable and large-size lithium batteries. Battery failure could result from or cause significant temperature rise within a battery. Thermal management [1] is crucial to the safe operation of, and the achievement of normal/optimal performance of electric vehicle batteries. Thermal mathematical modelling [2] has been widely applied to analyze lithium battery thermal performance under galvanostatic charge/discharge conditions [3–6]. A thermal analysis of lithium/polymer-electrolyte batteries during the Simplified Federal Urban Driving Schedule (SFUDS) dynamic power profile has been conducted by Chen and Evans [7,8] at Lawrence Berkeley National Laboratory (under the support of the US Department of Energy). The investigation provided information on thermal characteristics of batteries of this type, and guidelines for designing suitable thermal management systems. With the support of the United States Advanced Battery Consortium (USABC), Sandia National Laboratory (SNL) [9] conducted studies on the design and thermal analysis of lithium polymer batteries. As an additional part of the present work, heat generation rates within a battery during the USABC Dynamic Stress Test (DST) were calculated and compared with those during the SFUDS. Also, calculations of temperature rise in the C/Polymer electrolyte/$LiMn_2O_4$ batteries of Sandia conceptual designs for a Ford van and GM Impact, during a DST (to 80% DOD)/Fast Charge (put 40% of the total battery energy back in 1 h) /DST (to 80%DOD)/Full Charge (C/4) cycle, were conducted with a three-dimensional thermal model.

2. Conceptual battery designs

A conceptual battery design of the C/Polymer electrolyte/$LiMn_2O_4$ system for a Ford van consists of five modules [9]. Each module (monopolar design) is 28-cm high, 28-cm wide, and 31-cm long (each side of the module includes 1-cm thick

* Corresponding author.

PII S0378-7753(97)02679-7

polypropylene for packaging). Each module contains 20 series connected blocks of 38 parallel cells. Each cell is 20 × 20 cm. A 1-mil (25.4 μm) Cu anode current collector has 6-mil thick C (composite electrode) on each side, and a 1-mil Al cathode current collector has 6-mil thick $LiMn_2O_4$ (composite electrode) on each side. The polymer electrolyte separator is 2-mil thick. The battery design for the GM Impact also consists of five series-connected modules. Each module is 32-cm wide, 32-cm high, and 20.3-cm long. The packaging is 1-cm thick polypropylene. Each module contains 20-series-connected blocks of 38 parallel cells. Each cell is 30 × 30 cm. A 1-mil Cu anode collector has 3.5-mil thick C on each side. A 1 mil-Al cathode collector has 3 mil-thick $LiMn_2O_4$ on each side. The polymer electrolyte separator is 2-mil thick.

3. Thermophysical properties

Because of the shortage of the thermophysical properties data of some cell components, the following data from Refs. [10,11] are adopted in the present calculations.

C	Thermal conductivity	$k = 0.0205$ W cm^{-1} K^{-1} (petroleum coke)
	Density	$\rho = 1.55$ g cm^{-3} (petroleum coke)
	Specific heat	$C_p = 0.717$ J g^{-1} K^{-1} (graphite)
$LiMn_2O_4$	Thermal conductivity	$k = 0.0343$ W cm^{-1} K^{-1} (Mn_3O_4)
	Density	$\rho = 4.21$ g cm^{-3} (Mn_3O_4)
	Specific heat	$C_p = 0.6295$ J g^{-1} K^{-1} (MnO_2)

The thermophysical properties of the composite anode and cathode can be estimated in terms of the above data and the composition data of the electrodes.

Composition of composite electrode

Composite anode	C	50% (volume)	55.6% (mass)
	polymer electrolyte	50% (volume)	44.4% (mass)
Composite cathode	$LiMn_2O_4$	50% (volume)	80% (mass)
	polymer electrolyte	42% (volume)	16.1% (mass)
	C	8% (volume)	3.9% (mass)

Thermophysical properties of cell components

	k (W cm^{-1} K^{-1})	ρ (g cm^{-3})	C_p (J g^{-1} K^{-1})
Cu	3.98	8.96	0.385
Al	2.37	2.70	0.900
Polymer electrolyte	0.0016	1.20	2.050
Anode	0.0110	1.38	1.309
Cathode	0.0195	2.73	0.862

4. Mathematical model

In an electric vehicle, several battery modules are placed next to each other. However, under optimal conditions, a battery stack may be placed into an enclosure, and the stack is installed in such a way that convective air cooling can be made at the cooling channels among cell stacks and at the external surface of a stack. Therefore, heat transfer modelling can be made for the basic unit of a battery module, that is, a compact cell stack. Fig. 1 shows the schematic diagram of a battery module. The mathematical model has been described in reference [7]. In the present calculations, the heat transfer coefficient at cell stack surface is assumed to be 6 W m^{-2} K^{-1} for natural air flow, and 25 W m^{-2} K^{-1} for convective air flow.

5. Results and discussion

5.1. Heat generation rate during DST power profile, compared to that during SFUDS

Fig. 2 shows the USABC DST power profile [12] (solid line) and the SFUDS power profile [13] (dashed line). In consideration of the availability of the experimental charge/discharge data (at different rates), the Li/$P(EO)_8LiClO_4/TiS_2$ cell [14] is chosen in the present simulation.

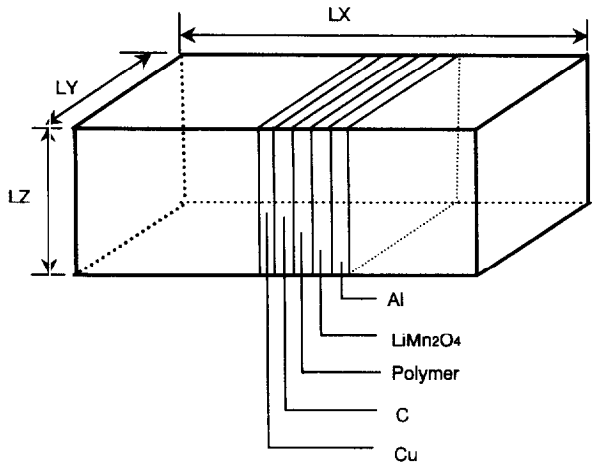

Fig. 1. Schematic of a battery module.

A monopolar design, which is a more mature design at the present stage of development (as compared with a bipolar design), is adopted. The thickness of each cell component is assumed to be: 25 μm [15] of Al current collector, 50 μm [16] of Li negative electrode, 50 μm [16] of polymer electrolyte, and 50 μm [16] of TiS_2 composite positive electrode. If package and other accessories are assumed to be 9% of the cell weight, the specific energy of the Li/TiS_2 cell under constant-current discharge (average voltage: 2.2 V) is estimated to be 62 W h kg^{-1} (for lithium/polymer batteries with V_6O_{13} as active material of the composite electrode, much higher specific energy, e.g., 200 W h kg^{-1}, may be achieved).

A simulation of the $Li/P(EO)_8LiClO_4/TiS_2$ battery predicts an operation time of 2.4 h under the DST profile (that is, 24 6-min DST subcycles), which is close to the operational time of a bipolar nickel–metal hydride battery [17] with similar specific energy. In other words, the simulation predicts a specific energy of 43 W h kg^{-1} during the DST dynamic power profile. After 2.4 h, the battery is unable to provide the maximum peak power of 120 W kg^{-1} (cell voltage drops below 1.4 V). A simulation of the battery during the SFUDS profile is also conducted, which predicts an operational time of 4.9 h and a specific energy of 56 W h kg^{-1}.

Fig. 3 shows the variation of cell voltage, current density, and heat generation rate during the final 6-min subcycle of the DST profile. Fig. 4 presents the heat generation rates during the whole battery operation process under the DST profile. It can be seen that the maximum heat generation rate at the initial stage (high state of charge) of battery operation corresponds to the regenerative braking at the 60 W kg^{-1} power level, while as the battery operation proceeds, heat generation rate during the maximum power extraction of 120 W kg^{-1} increases significantly (especially at high depth of discharge). Fig. 5 shows a comparison of heat generation rates at the end of battery operation during the DST profile and the SFUDS profile. Fig. 6 shows the heat generation rate averaged over each 6-min subcycle during the two dynamic power profiles. As would be expected, the heat generation rate during the DST profile is much higher than that during the SFUDS profile. The total

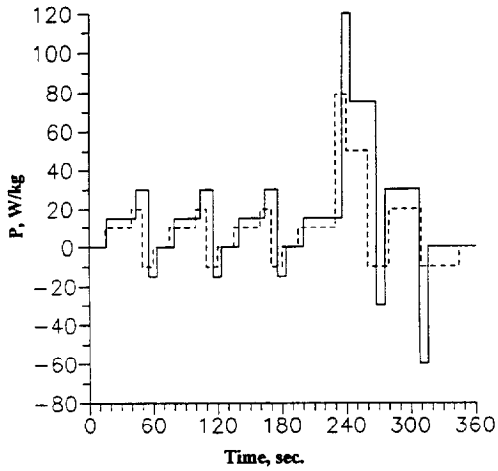

Fig. 2. DST (———) and SFUDS (- - -) power profile (negative powers correspond to charging during regenerative braking).

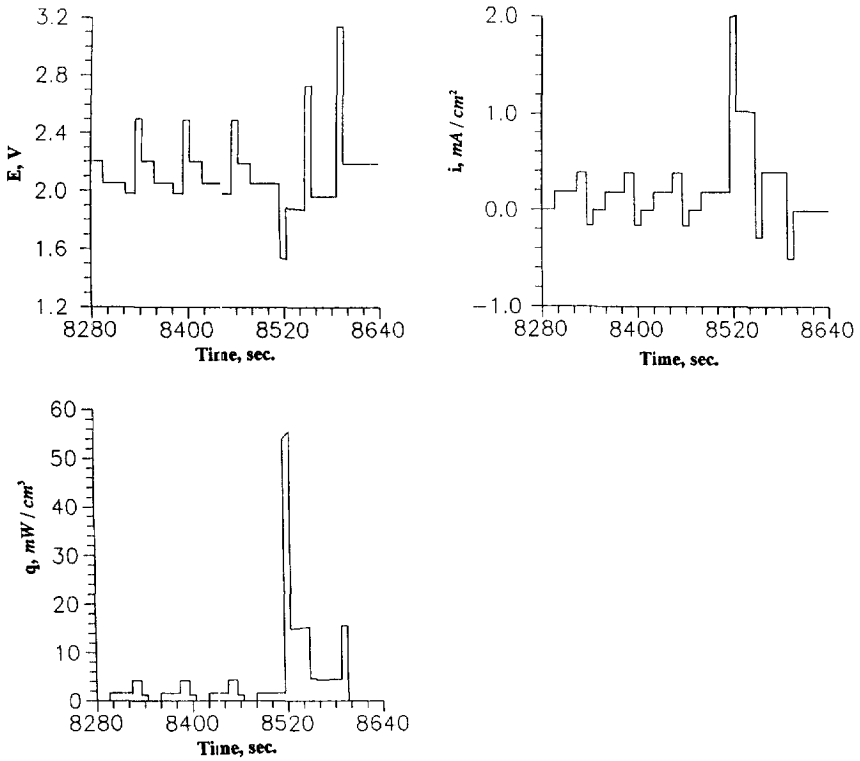

Fig. 3. Variation of cell voltage, current density, and heat generation rate in a Li/TiS_2 cell during the final 6-min subcycle of the DST power profile.

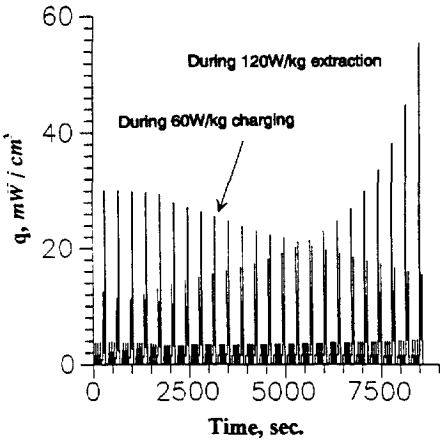

Fig. 4. Heat generation rate in a Li/TiS_2 cell during the DST power profile.

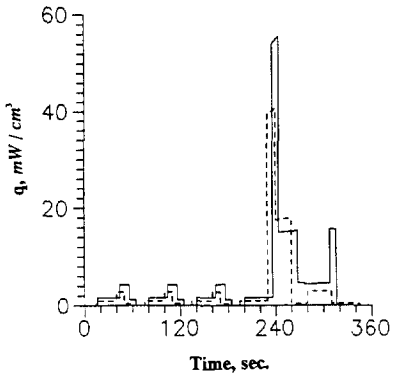

Fig. 5. Comparison of heat generation rate during the final 6-min subcycle of the DST (———) and SFUDS (---) power profile.

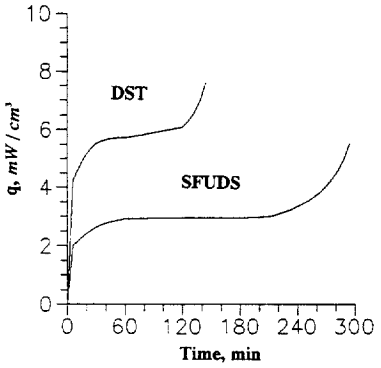

Fig. 6. Heat generation rate averaged over each 6-min subcycle During the DST and SFUDS power profile.

heat generation is 15.7% of the energy initially stored in the battery during the DST profile, and 13.6% during the SFUDS profile, respectively.

5.2. Temperature rise in the batteries of the Sandia conceptual designs

In discharge of all practical batteries, heat generation rate will increase with the increasing depth of discharge and charge/discharge rate. However, in many cases, due to the shortage of experimental charge/discharge data (at different rates), and for simplicity, a constant heat generation rate during the a dynamic power profile may be assumed. Fig. 7 shows the percentage of heat generation in the total energy (delivered electric energy plus heat) obtained from a $Li/P(EO)_8LiClO_4/TiS_2$ cell as a function of constant current discharge rate (C-rate). It can be seen that the battery energy efficiency is from 70% to 90% during a single discharge process. In many cases, it is widely assumed that heat generation is about 10% of the electric energy of the battery on both charge and discharge at low or medium rates (e.g., C/3). Under this assumption, for the C/Polymer electrolyte/$LiMn_2O_4$ batteries, the corresponding heat generation rate may be estimated according to the following simple expression,

$$q = 10\%(P \cdot \rho)$$

q: heat generation rate (W cm^{-3}); P: power (W kg^{-1}); ρ: module density (kg cm^{-3}); 1.96×10^{-3} kg cm^{-3} for the Ford van battery module; 1.98×10^{-3} kg cm^{-3} for the GM Impact battery module.

The full discharge power in the DST profile is chosen to be 120 W kg^{-1} (see Fig. 2), namely, 80% of the USABC midterm goal of 150 W kg^{-1}. Therefore, heat generation rates for different power levels of the DST profile (see Fig. 2) are shown below.

	Discharge				Charge		
Power (W kg^{-1})	15	30	75	120	−15	−30	−60
Heat generation rate (mW cm^{-3})	2.94	5.88	14.70	23.52	2.94	5.88	11.76

Heat will be generated during both discharge and charge process, and the average heat generation rate during the DST power profile is 4.12 mW cm^{-3}. During each 6-min subcycle of the DST profile, the extraction of specific energy is 1.8 W

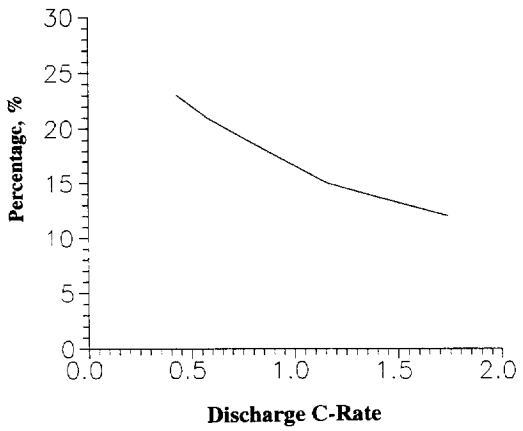

Fig. 7. Percentage of heat generation in total battery energy as a function of constant-current discharge rate of a Li/TiS_2 cell.

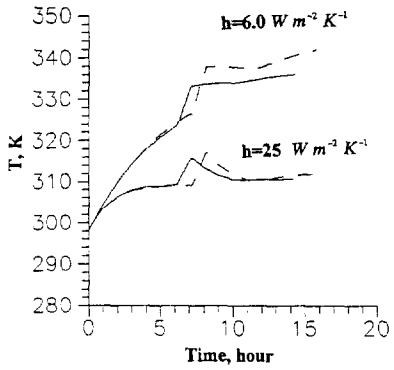

Fig. 8. Variation of temperature at module center during one cycle consisting of DST/1-h fast charge/DST/4-h full charge: battery for GM Impact (———), battery for Ford Van (---).

h kg^{-1}. The specific energy returned to the battery through regenerative braking is 0.3 W h kg^{-1}. The net energy extraction during each 6-min subcycle of the DST profile is 1.50 W h kg^{-1}. The specific energy of the conceptual battery designs for the Ford van and GM Impact is 134 W h kg^{-1} and 116 W h kg^{-1}, respectively. If the depth of discharge is 80%, the battery operation time (after a full charge) under the DST profile is 6.44 h and 5.57 h, for the Ford van and GM Impact batteries, respectively.

If 40% of the battery energy is put back by a 1-h fast charge, the heat generation rate (10% of the passed energy) is 10.36 mW cm^{-3} and 9.19 mW cm^{-3}, respectively for the Ford van and GM Impact batteries. Similarly, if full charge is realized over a 4-h period, the heat generation rates within the two batteries are estimated to be 5.18 mW cm^{-3} and 4.60 mW cm^{-3}.

Fig. 8 shows the temperature rise at the center of a battery module during a cycle consisting of DST/1-h Fast Charge/DST/4-h Full Charge, for two cooling conditions. The solid line is for the GM Impact battery, while the dashed line is for the Ford van battery. Under natural air flow condition (h = 6 W m^{-2} K^{-1}), the predicted temperature rise at the end of one cycle is 38°C in the GM battery, and 44°C in the Ford battery, that is, battery temperature reaches 63°C and 69°C, respectively. If convective air cooling is applied, the corresponding temperature rise is 13°C and 14°C, respectively. Because the battery operational time is long (e.g., over 5 h from full charge to 80% DOD under the DST profile, if the 120 W kg^{-1} of peak power can be obtained at 80% DOD for the battery), the convective air cooling is expected to be effective in reducing battery temperature at the end of one cycle, although rapid temperature increase is caused during the 1-h fast charging.

6. Summary

Heat generation rate in a Li/$P(EO)_8LiClO_4$/TiS_2 cell during the DST profile has been examined and compared with that during the SFUDS profile. The heat generation is significantly greater for the former profile with correspondingly lower specific energy. Also, the calculations of the temperature rise in the Sandia conceptual battery designs of C/Polymer electrolyte/$LiMn_2O_4$ batteries for a Ford van and GM Impact have been conducted, indicating the need for convective cooling to avoid significant temperature increase in the batteries. The analysis of this paper provides a methodology for examining battery thermal behaviour under dynamic power profiles.

Acknowledgements

This work was supported by the Assistant Secretary for Energy Efficiency and Renewable Energy, Office of Transportation Technologies, Office of Advanced Automotive Technologies of the U.S. Department of Energy under Contract No. DE-AC03-76SF00098. The United States Advanced Battery Consortium is thanked for permission to publish details of the Sandia designs.

References

[1] H.F. Gibbard, C.C. Chen, Thermal Management of Batteries, in: J. Thompson (Ed.), Power Sources, vol. 8, Academic Press, New York, 1981, p. 263.
[2] J. Lee, Battery Thermal Modelling, The Methodology and Applications, in: J.R. Selman, H.C. Maru (Eds.), Electrochemical and Thermal Modelling of Battery, Fuel Cell and Photoenergy Conversion Systems, PV86-12, The Electrochemical Society, Pennington, NJ, 1986, p. 206.

[3] J. Newman, W. Tiedemann, Temperature rise in a battery module with constant heat generation, J. Electrochem. Soc. 142 (1995) 1054.
[4] M.W. Verbrugge, Three-dimensional temperature and current distribution in a battery module, AIChE J. 41 (1995) 1550.
[5] C.R. Pals, J. Newman, Thermal modelling of the lithium/polymer battery: I. Discharge behaviour of a single cell, J. Electrochem. Soc. 142 (1995) 3274.
[6] C.R. Pals, J. Newman, Thermal modelling of the lithium/polymer battery: II. Temperature profiles in a cell stack, J. Electrochem. Soc. 142 (1995) 3282.
[7] Y. Chen, J.W. Evans, Three-dimensional thermal modelling of lithium/polymer batteries under galvanostatic discharge and dynamic power profile, J. Electrochem. Soc. 141 (1994) 2947.
[8] Y. Chen, J.W. Evans, Thermal Management of Lithium/Polymer-Electrolyte Batteries for Electric Vehicle Application, in: S. Megahed, B. Barnett, L. Xie (Eds.), Rechargeable Lithium and Lithium-Ion Batteries, PV94-28, The Electrochemical Society, Pennington, NJ, 1994, p. 73.
[9] G. Scharrer et al., Sandia National Laboratory/United States Advanced Battery Consortium (USABC) Task 4, Internal Report, 1994.
[10] Y.S. Touloukian, R.W. Powell, C.Y. Ho, P.G. Klemens (Eds.), Thermophysical Properties of Matter, vol. 2, Thermal Conductivity: Nonmetallic Solids, IFI/Plenum, New York, 1970.
[11] Y.S. Touloukian, E.H. Buyco (Eds.), Thermophysical Properties of Matter, vol. 5, Specific Heat: Nonmetallic Solids, IFI/Plenum, New York, 1970.
[12] Electric Vehicle Battery Test Procedures Manual, United States Advanced battery Consortium, July, 1994.
[13] A Simplified Version of the Federal Urban Driving Schedule for Electric Vehicle Battery Testing, Electric and Hybrid Propulsion Battery Test Working Force, EG and G, Idaho, DOE/ID-10146, 1988.
[14] M. Gauthier, D. Fauteux, G. Vassort, A. Belanger, M. Duval, P. Ricoux, J.M. Chabagno, D. Muller, P. Rigaud, M.B. Armand, D. Deroo, Assessment of polymer-electrolyte batteries for EV and ambient temperature applications, J. Electrochem. Soc. 132 (1985) 1333.
[15] M.Z.A. Munshi, B.B. Owens, Assessment of thin film batteries based on polymer electrolytes: I. Energy density, Solid State Ionics 38 (1990) 87.
[16] C.D.S. Tuck, (Ed.), Modern Battery Technology, Ellis Horwood, England, 1991, p. 529.
[17] D.E. Reisner, M. Klein, Cell Design and Evaluation for Low-Cost Bipolar Nickel–Metal Hydride EV Battery, in: Proc. 29th Intersociety Energy Conversion Engineering Conference, Monterey, CA, Aug. 7–11, 1994, p. 780.